Journal of Solid State Chemistry 184 (2011) 1465–1471

Contents lists available at ScienceDirect

Journal of Solid State Chemistry

journal homepage: www.elsevier.com/locate/jssc

# $TiO_2$/carbon nanotube hybrid nanostructures: Solvothermal synthesis and their visible light photocatalytic activity

Lihong Tian [a,b], Liqun Ye [a], Kejian Deng [c], Ling Zan [a,*]

[a] College of Chemistry and Molecular Sciences, Wuhan University, Wuhan 430072, P.R. China
[b] College of Chemistry & Chemical Engineering, Hubei University, Wuhan 430062, P.R. China
[c] Key Laboratory of Catalysis and Materials Science of the State Ethnic Affairs Commission and Ministry of Education, South-Central University for Nationalities, Wuhan 430074, P.R. China

ARTICLE INFO

*Article history:*
Received 30 November 2010
Received in revised form
30 March 2011
Accepted 6 April 2011
Available online 15 April 2011

*Keywords:*
$TiO_2$/MWCNTs
Hybrid materials
Ti–C bond
Photocatalytic degradation.

ABSTRACT

MWCNT/$TiO_2$ hybrid nanostructures were prepared via solvothermal synthesis and sol–gel method with benzyl alcohol as a surfactant. As-prepared hybrid materials were characterized by X-ray diffraction, transmission electron microscopy, UV–vis diffuse reflectance spectra and X-ray photoelectron spectroscopy. The results showed that MWCNTs were uniformly decorated with anatase nanocrystals in solvothermal condition, but MWCNTs were embedded in a majority of $TiO_2$ nanoparticles by sol–gel method. When the weight ratio of MWCNTs to $TiO_2$ was 20%, MWCNT/$TiO_2$ hybrid nanostructures prepared by solvothermal synthesis exhibited higher visible-light-driven photocatalytic activity than that prepared by sol–gel method. Post-annealing of MWCNT/$TiO_2$ nanostructures at 400 °C resulted in the formation of the carbonaceous Ti–C bonds on the interface between $TiO_2$ and MWCNTs, which enhanced the photoabsorbance of the hybrid materials in the visible light region and improved the visible-light degradation efficiency of methylene blue.



## 1. Introduction

Semiconductor photocatalysts have attracted many researchers' attention in the past decades for their potential applications in environmental purification and solar energy conversion. Among abundant photocatalysts, $TiO_2$ is probably the most promising owing to its superior photocatalytic activity, and physical and chemical properties [1–3]. However, the wide band-gaps (3.0–3.2 eV) and high recombination rate of electron–holes in anatase and/or rutile $TiO_2$ photocatalysts give rise to a low quantum efficiency of photocatalytic reactions. It is interesting to extend the photo-response into visible light region and to promote the commercial application of the titanium dioxide-based materials. To date, substantial efforts have been made to attain this objective, such as doping with transition metals or nonmetal elements [4–7], coupling with secondary semiconductors and photosensitization of dye and so forth [8–10].

CNTs/$TiO_2$ nanostructures have been considered as a good photocatalyst candidate because of their large surface area and excellent charge transfer ability. Carbon nanotube has a variety of electronic properties and one of its' many possible electronic structures is similar to the metals, namely, exhibiting metallic conductivity [11]. The conductive structure of the CNTs is believed to accept and transfer the UV-light excited electrons from the conduction band of $TiO_2$ to the CNTs surface and decrease the possibility of the recombination of the electron–hole pairs, causing quicker degradation of the target molecules [12–22]. For example, Gao et. al. [20] recently demonstrated that the MWCNTs could be uniformly coated with anatase $TiO_2$ by a surfactant wrapping sol–gel method, and the photocatalytic activity on decomposing the methylene blue under UV-light irradiation was enhanced. Xu et al. [21] synthesized the $TiO_2$/MWCNT nanocomposite by a simple wet impregnation method, which showed the improved photocatalytic performance for the application to both liquid- and gas-phase environmental cleanups.

In previous investigations, most studies were focused on the photocatalytic reactions of $TiO_2$/MWCNT composite materials under UV-light irradiation; only a few reports were on the visible light-driven photodegradation of pollutants using $TiO_2$/MWCNT hybrid materials. The photocatalytic mechanism of pollutants on visible light-driven $TiO_2$/MWCNT hybrids is still not clear [15,23,24]. Recently, non-hydrolytic route has attracted increasing attention for the preparation of hybrid materials [25,26]. In this paper, MWCNT/$TiO_2$ hybrid nanostructures were fabricated by solvothermal method in ethanol solvent. The morphology and interface interaction of MWCNT/$TiO_2$ hybrids were investigated by TEM, XPS and UV–visible absorption. The photocatalytic activity of MWCNT/$TiO_2$ hybrid materials towards methylene blue degradation under visible light irradiation was studied, as methylene blue was

* Corresponding author. Fax: +86 27 87378727.
*E-mail address:* irlab@whu.edu.cn (L. Zan).

0022-4596/$ - see front matter Crown Copyright © 2011 Published by Elsevier Inc. All rights reserved.
doi:10.1016/j.jssc.2011.04.014

the usual reactant to test the photocatalytic power of various hybrid nanostructures [27,28]. Comparing the photocatalytic activity of MWCNT/$TiO_2$ hybrid structures prepared by different methods with the mechanical mixture of MWCNTs and $TiO_2$, we attempt to find the relationship between morphological structure, bonding interaction of MWCNT/$TiO_2$ nanostructures and visible-light induced photocatalytic activity.

## 2. Experimental section

### 2.1. Preparation of MWCNT/$TiO_2$ hybrid nanostructures via solvothermal route

Multi-wall carbon nanotubes (MWCNTs, purity $>95$ wt%; diameter: 30–50 nm; length: about 20 μm; specific surface area $>60\ m^2/g$) were purchased from Chengdu Organic Chemicals Co. Ltd., Chinese Academy of Sciences. $TiCl_4$ ($\geq 98.0\%$, C.P., Sinopharm Chemical Reagent Co., Ltd) and anhydrous ethanol ($\geq 99.7\%$, Sinopharm Chemical Reagent Co., Ltd) were used without further purification. In typical experiment, MWCNTs were oxidized by refluxing at 120 °C in mixed acid ($H_2SO_4$:$HNO_3$=3:1) for 30 min and then the mixture was diluted with water and filtered. The obtained samples were washed by water to obtain pH=7 and dried in the oven at 60 °C for 12 h. The MWCNT/$TiO_2$ hybrid nanostructures were prepared from titanium chloride by solvothermal method. Briefly, 0.5 mL $TiCl_4$ (4.55 mmol) was slowly dropped into 40 mL ethanol and stirred magnetically to provide a completely transparent yellow solution. A desired amount of MWCNTs were dissolved and ultrasonically dispersed in the solution. Then it was transferred into a Teflon-lined, stainless autoclave and stored at 120 °C for 24 h, producing the gray or dark precipitate. The precipitate was separated by centrifugation and washed carefully with anhydrous ethanol (3 × 20 mL) to remove organic species. The collected materials were left to dry in an oven at 60 °C for 12 h, then calcined at different temperature (100–400 °C) for 2 h to obtain the MWCNT/$TiO_2$ hybrid nanostructures. The sample was assigned as ST-MWCNT/$TiO_2$ (wt%), here, wt% is the weight ratio of MWCNTs to $TiO_2$. The pure $TiO_2$ powders were prepared in a similar procedure. The mechanical mixtures of MWCNTs and $TiO_2$ were prepared by mixing the proportional MWCNT and $TiO_2$ particles in a mortar. Generally, the samples contain 20% CNT unless stated in this paper.

### 2.2. Preparation of MWCNT/$TiO_2$ nanostructures by sol–gel method

In this work, MWCNT/$TiO_2$ nanostructure was also synthesized by modified sol–gel method using benzyl alcohol as a surfactant [29]. Typically, 45 mg acid-treated MWCNTs were dispersed in 14 mL ethanol solution with the aid of ultrasonication for 30 min, then 1.5 mL benzyl alcohol and 0.25 mL $H_2O$ were added. The solution was magnetically stirred at 0 °C; 1 mL $Ti(OBu)_4$ was dissolved in 3 mL ethanol and slowly dropped into the CNTs suspension. After stirred for 1 h at 0 °C, the dark precipitates were vacuum-filtered, washed in ethanol (10 mL × 3) and dried in air at 60 °C. The final powders were calcined at 400 °C for 2 h to crystallize the $TiO_2$ and obtain MWCNT/$TiO_2$ composite containing 20% CNTs, which was noted as SG-MWCNT/$TiO_2$ (20%).

### 2.3. Characterization

The samples were examined by X-ray diffraction analysis, and performed on the Bruker D8 advance X-ray diffractometer with Cu$K\alpha$ radiation (1.5406 Å). The morphologies were studied by a transmission electron microscopy, operating at accelerating voltage of 200 kV with a tungsten filament (FFI Tecnai G20). X-ray photoelectron spectroscopy (XPS) measurements were carried out on VG Multilab 2000 spectrometer with an ALKa X-ray source (Thermo Electron Corporation), and all the spectra were calibrated to the C 1*s* peak at 284.4 eV. The UV–visible diffuse reflection spectra were obtained for the dry-pressed disk samples on a UV–vis spectrophotometer (UV-3600) with $BaSO_4$ as the reflectance sample. Intermediate compounds of the degradation of methylene blue were identified by GC/MS (Varian 450GC-320MS). The column temperature program was: 313 K (2 min) and 313–473 K (5 K $min^{-1}$, hold time: 10 min).

### 2.4. Photocatalytic degradation of methylene blue

The photocatalytic degradation of methylene blue (MB, aqueous solution was performed under visible light irradiation using a high-pressure halogen lamp (500 W) with UV light filter, which transmitted light at a wavelength $>420$ nm. Typically, 20 mg of photocatalyst was suspended in an aqueous solution (100 mL) containing 10 mg/L MB dye by sonication for 10 min and magnetically stirred for 1 h in the dark room to ensure that the adsorption/desorption equilibrium of the dye on the catalyst surface was established. The solution was placed in a quartz reaction vessel and stirred with a magnetic stirrer. A circulating water jacket was employed to cool the solution and thus keep the temperature of the solution constant. A liquid (5 mL) was sampled at scheduled irradiation time and the suspended catalysts were removed by centrifugation and separation. The UV–visible absorption spectrum of the solution was measured using a UV–vis spectrophotometer (UV-3600). The percentage of degradation was reported as $C/C_0$, here, $C_0$ is the absorption ($\lambda_{max}$=664 nm) of methylene blue solution before irradiation and $C$ is the absorption of methylene blue solution at each irradiated time interval.

## 3. Results and discussion

### 3.1. XRD analysis

The XRD patterns were examined in order to investigate the effect of MWCNTs content on the crystallinity of the hybrids (ST-MWCNT/$TiO_2$). The diffraction peak at $2\theta$ value of 26.1° is assigned to the (002) plane of the CNT (Fig. 1a). The XRD patterns of MWCNT/$TiO_2$ hybrid nanostructures with different contents of CNTs and the mechanical mixture of $TiO_2$ and CNTs demonstrate the obvious crystalline nature (Fig. 1c–f). Some diffraction peaks at 25.4°, 37.9°, 48.1°, 53.9° and 62.8° can be attributed to the (101), (004), (200), (105) and (204) crystal planes of anatase $TiO_2$ (JCPDS no. 21-1272), respectively. Notably, the characteristic peak for CNTs at 26.1° is absent in these MWCNT/$TiO_2$ hybrid nanostructures, which is due to the fact that the characteristic peak of CNTs might be shielded by the main peak of anatase $TiO_2$ at 25.4° because of the low content of CNTs in MWCNT/$TiO_2$ hybrid nanostructures [30]. The XRD pattern of SG-MWCNTs/$TiO_2$ (20%) nanostructures is displayed in Fig.1b. Clearly, all the diffraction peaks correspond to anatase phase of $TiO_2$. Compared with that of ST-MWCNT/$TiO_2$ (20%), the intensity of peaks is weaker and the width of main peak broadens for SG-MWCNTs/$TiO_2$ (20%), which indicates that smaller $TiO_2$ nanoparticles were obtained by sol–gel method because benzyl alcohol as a surfactant enables keeping the particle size small by sol–gel method [31].

### 3.2. Morphology and structure

TEM images (Fig. 2) illustrated the morphologies of the MWCNT/$TiO_2$ hybrid nanostructures with different weight ratios

of CNTs to $TiO_2$. Fig. 2a shows the TEM image of ST-MWCNT/$TiO_2$ hybrid materials with CNTs content of 10%; it can be seen that a few $TiO_2$ nanocrystals attach on the surface of CNT, and a cluster of $TiO_2$ particles is observed. In the sample containing 20% CNTs, the uniform and dense $TiO_2$ nanocrystals attach on the CNTs surface and the size of particles is about 5–14 nm (Fig. 2b). This may indicate that CNTs promoted the dispersion of $TiO_2$ particles in solvothermal process, which conforms to Zhang's report [32]. However, when the content of CNTs reached 25%, a number of $TiO_2$ nanocrystals aggregated on the surface of twisted MWCNTs (Fig. 2c). For SG-MWCNT/$TiO_2$ nanostructures, the morphology is different from that of the ST-MWCNT/$TiO_2$ hybrid material; CNTs are embedded in aggregated $TiO_2$ nanoparticles and the particle size of $TiO_2$ is about 7 nm in the presence of surfactant by sol–gel method (Fig. 2d). The results indicated that CNTs only acted as the supports and are coated by hydrolysis products and $TiO_2$ nanoparticles aggregated on the surface of CNTs in sol–gel system. However, in the solvothermal reaction, the high pressure and temperature probably facilitated the dispersions of CNTs in solvent and nucleation of $TiO_2$ on CNTs surface, which result in the uniform decoration of $TiO_2$ nanoparticles on CNTs.

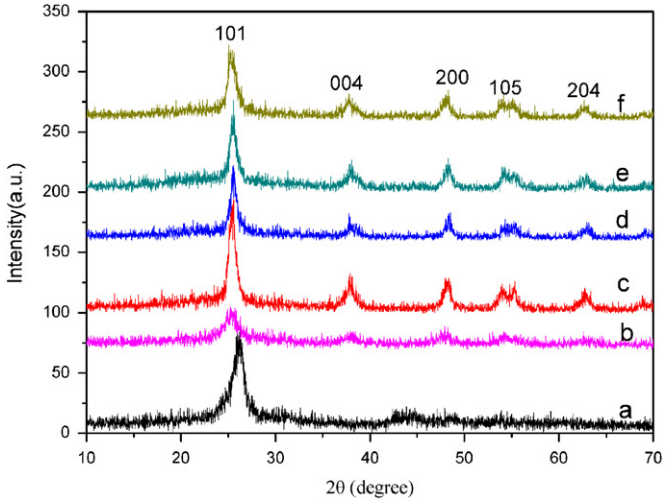


**Fig.1.** XRD patterns of pure MWCNTs and MWCNT/$TiO_2$ hybrid nanostructures. (a) pure MWCNTs, (b) SG-MWCNT/$TiO_2$ (20%), (c) ST-MWCNT/$TiO_2$ (10%), (d) ST-MWCNT/$TiO_2$ (20%) and (e) ST-MWCNT/$TiO_2$ (25%) and (f) the mechanical mixture of $TiO_2$ and MWCNTs.

### 3.3. XPS and DRS analyses

Fig. 3 shows the C1*s* XPS spectra for acid-treated MWCNTs and ST-MWCNT/$TiO_2$ (20%) calcined at 400 °C. In Fig. 3a, the C1*s* peak at 284.4 eV is ascribed to C–C bonds of MWCNTs; the peaks at 285.1 and 289.8 eV are assigned to C–O and COO bonds, respectively [23], which indicated acid-treated CNTs had abundant of hydrophilic groups such as C–OH or –COOH on the surface. These groups not only help to disperse MWCNTs in ethanol well but also facilitate the adsorption of $TiCl_4$ precursor molecules on the CNTs surface. In contrast to the acid-treated CNTs, a new peak appears

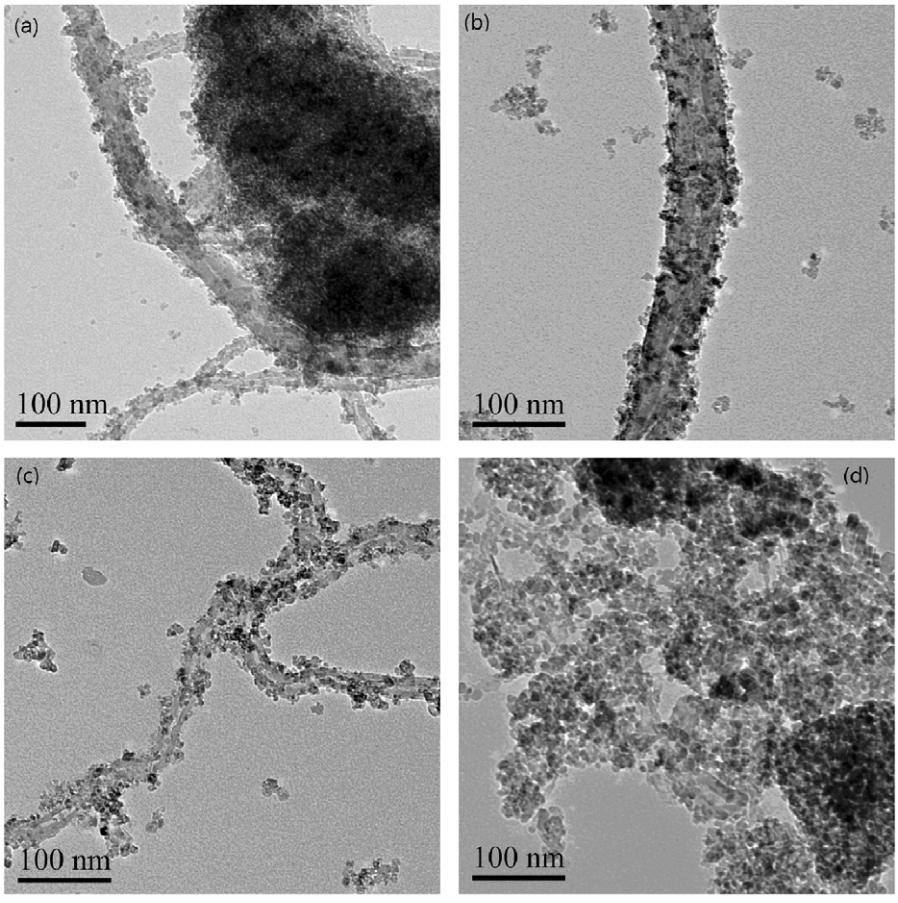


**Fig. 2.** TEM micrographs of MWCNT/$TiO_2$ hybrid nanostructures with different contents of CNTs. (a) ST-MWCNT/$TiO_2$ (10%), (b) ST-MWCNT/$TiO_2$ (20%), (c) ST-MWCNT/$TiO_2$ (25%) and (d) SG-MWCNT/$TiO_2$ (20%).

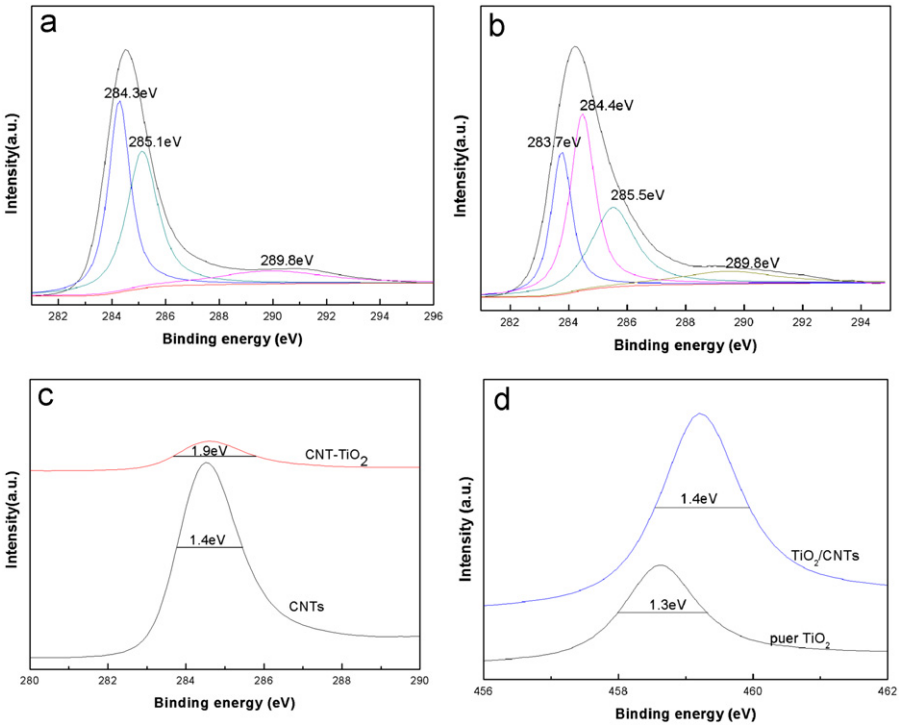


**Fig. 3.** XPS spectra: (a) C1*s* spectra of pure MWCNTs, (b) C1*s* spectra of ST-$TiO_2$/MWCNTs (20%), (c) C1*s* FWHM contrast centered at 284.4 eV of pure CNTs and ST-$TiO_2$/MWCNTs (20%) and (d) Ti $2p_{3/2}$ FWHM contrast of ST-$TiO_2$/MWCNTs (20%) and pure $TiO_2$.

at 283.7 eV for ST-MWCNT/$TiO_2$ (20%), which is ascribed to the Ti–C carbonaceous bond (Fig. 3b) [33–35]. In addition, it is clearly displayed in Fig. 3c, as the $TiO_2$ nanocrystals depositing on CNTs, the C1*s* full-width at half-maxinum (FWHM) of the asymmetric band, centered at 284.4 eV, increases from 1.4 to 1.9 eV. Ti $2p_{3/2}$ and Ti $2p_{1/2}$ spin–orbital splitting photoelectrons of hybrids are 459.2 and 464.9 eV, respectively, which slightly shift towards higher binding energy compared with those of the pure anatase $TiO_2$ (not shown here) [36]. Fig. 3d displays the Ti $2p_{3/2}$ peaks of pure $TiO_2$ and MWCNT/$TiO_2$ hybrid nanostructures. As the $TiO_2$ nanocrystals were deposited on CNTs, the peaks became broader and the FWHM values increased from 1.3 to 1.4 eV. The results indicated the bonding interaction between CNTs and $TiO_2$ nanocrystals on MWCNT/$TiO_2$ interface [37]. However, for ST-MWCNT/$TiO_2$ (20%) calcined at 200 °C, no peak ascribed to Ti–C bond (not shown here) was found in its C1*s* spectrum. Post-annealing at 400 °C was essential for the formation of Ti–C bonds on MWCNT/$TiO_2$ interface. Yu's paper also indicated that the annealing temperature of 400 °C was necessary for the connection between CNTs and $TiO_2$ on their interface [38].

Fig. 4 shows the UV–vis DRS spectra for pure $TiO_2$, the mechanical mixture of $TiO_2$ and CNTs, ST-MWCNT/$TiO_2$ (20%) and pure CNTs. It can be seen that the fundamental absorbance edge of pure anatase $TiO_2$ is at 398 nm and has a little visible light absorption in its characteristic spectrum (curve a). Pure CNTs display strong photoabsorbance over the entire region from 300 to 600 nm (curve d). For the mixture of $TiO_2$ and CNTs, the absorption in the visible light region was associated with the absorption of the CNTs. Nevertheless, a strong absorption covers the whole visible light region for MWCNT/$TiO_2$ hybrid nanostructures, which is higher than that of the mechanical mixture of $TiO_2$ and CNTs in the wavelength range of 400–600 nm (curve c). According to the XPS results, the enhanced absorption of MWCNT/$TiO_2$ hybrid nanostructures in visible light range was attributed to the presence of Ti–C bonds in the interphase of MWCNT/$TiO_2$ hybrid nanostructures.

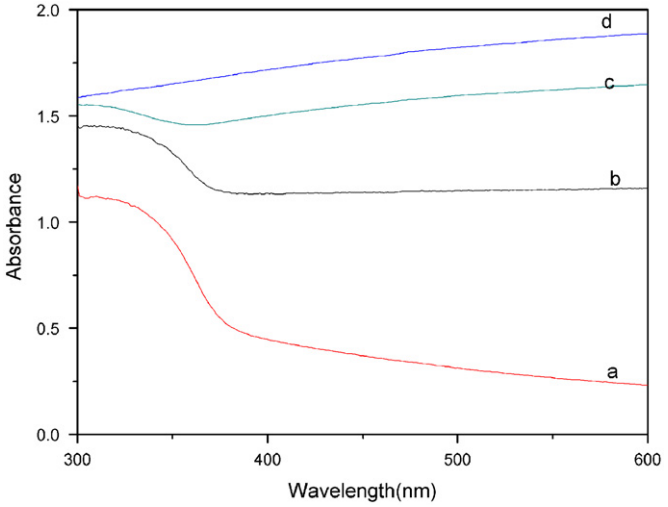


**Fig. 4.** UV–vis diffuse reflectance spectra of (a) pure $TiO_2$, (b) mixture of $TiO_2$ and MWCNTs (20%) (c) ST-MWCNT/$TiO_2$ (20%) and (d) bare CNTs.

### 3.4. Photocatalytic activity of MWCNT/$TiO_2$ hybrid nanostructures

#### 3.4.1. Effect of morphology

It is well-known that the photocatalytic activity of nano-materials strongly depends on their morphological structure [39–41]. The photocatalytic activity of MWCNT/$TiO_2$ hybrid nanostructures with different CNTs content has been investigated towards MB degradation under visible-light irradiation. Herein, Fig. 5 shows degradation rate of MB on ST-MWCNT/$TiO_2$ surface with different CNTs content. The concentration of methylene blue was determined according to the characteristic peak at around 664 nm in the UV–vis spectra. The best degradation effect was found at 20% of CNTs content. This leads to a judgment that uniform distribution of $TiO_2$ nanocrystals on CNTs surface (Fig. 2b) is an important factor to enhance the

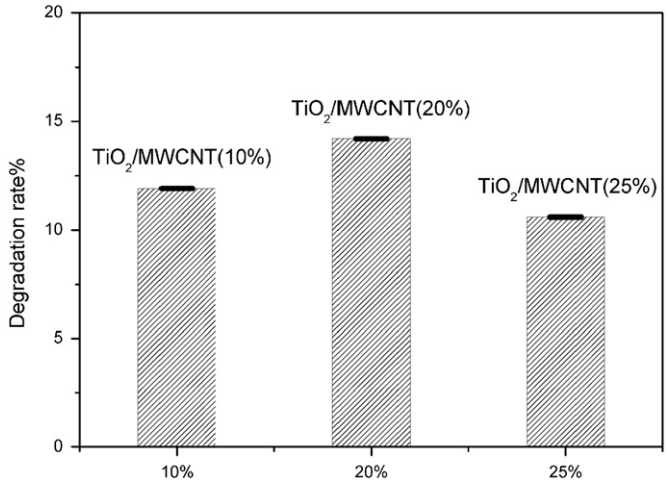


**Fig. 5.** Photodegradation rate of MB on ST-$TiO_2$/MWCNT hybrid nanostructures with different contents of CNTs. Experimental conditions: [MB]=5 mg/L, [photocatalysts]=0.1 g/L.

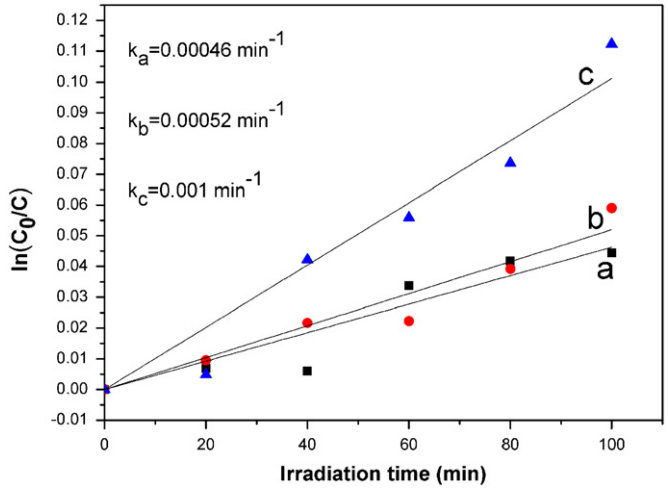


**Fig. 6.** The first-order kinetic plots of MB degradation on various CNT/$TiO_2$ hybrid nanostructures annealed at different temperatures under visible light irradiation (a) 60 °C, (b) 200 °C and (c) 400 °C. Experimental conditions: [MB]=10 mg/L, [photocatalysts]=0.2 g/L.

photocatalytic activity of MWCNT/$TiO_2$ hybrid nanostructures. Other morphology, such as the aggregation of nanoparticles, may hamper the electron transfer, and the excess of CNTs shields the light absorption of hybrid nanostructures.

### 3.4.2. *Effect of bonding interaction of hybrid nanostructures*

In order to investigate the effect of bonding interaction of MWCNT/$TiO_2$ hybrid material on its photocatalytic activity, the photocatalytic degradation of MB dye with various catalysts was carried out under visible light illumination ($\lambda$420 nm). On the basis of previous studies, the degradation of dyes can be ascribed to a pseudo-first-order reaction with a simplified Langmuir–Hinshelwood model when $C_0$ is very small: $\ln(C_0/C)=kt$, where $k$ is the apparent first-order rate constant [39]. Fig. 6 shows the first-order kinetic plots of MB degradation on various catalysts surface annealed at different temperatures. For ST-MWCNT/$TiO_2$ hybrid nanostructures (20%), the rate constant of MB degradation in the dispersion of photocatalysts annealed at 400 °C was twice of that in dispersion of photocatalysts annealed at 200 °C under

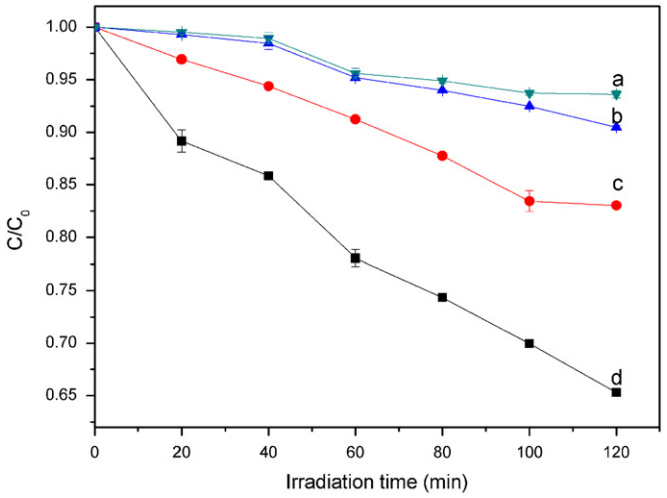


**Fig. 7.** Photocatalytic activity for MB solution of different catalysts under visible light irradiation: (a) mixture of $TiO_2$ and MWCNTs (20%), (b) pure $TiO_2$, (c) SG-MWCNT/$TiO_2$(20%) and (d) ST-MWCNT/$TiO_2$ (20%). Experimental conditions: [MB]=10 mg/L, [photocatalysts]=0.2 g/L.

visible light irradiation. The improvement in visible-light induced phtocatalytic activity of ST-MWCNT/$TiO_2$ annealed at 400 °C, compared with the ST-MWCNT/$TiO_2$ annealed at 200 °C, is a proof of the formation of Ti–C bond between the CNTs and the $TiO_2$ nanocrystals.

Fig. 7 shows the change of the concentration of MB with different irradiation times in various photocatalysts dispersions. The SG-MWCNT/$TiO_2$ (20%) significantly enhances the degradation of MB, compared with the pure $TiO_2$ and the mechanical mixture of MWCNTs and $TiO_2$. However, owing to the uniform distribution of $TiO_2$ nanocrystals on CNTs surface (Fig. 2b) the ST-MWCNT/$TiO_2$ (20%) possesses even higher photocatalytic activity than SG-MWCNT/$TiO_2$ (20%). There are several possible reasons for this enhancement: (1) the MWCNTs have excellent charge transfer ability, (2) the MWCNT/$TiO_2$ hybrid nanostructure has high surface area and increases the adsorption of MB on photocatalysts surface and (3) the Ti–C bonds between CNTs and $TiO_2$ promote the visible light absorption.

## 3.5. *Discussion of the formation mechanism of MWCNT/$TiO_2$ hybrid nanostructures*

The formation mechanism of MWCNT/$TiO_2$ hybrid nanostructures in solvothermal process is relatively complicated. The surface of acid-treated MWCNTs contained many C–O and –COOH groups, which have been revealed by XPS results. The polar groups were favorable to the adsorption of $TiCl_4$ precursor on the surface of MWCNTs. Further, supercritical ethanol in solvothermal process facilitated the adsorption of precursor on MWCNTs [15]. The nucleation and crystallization occurred on the MWCNTs surface by the ether-elimination reaction [40]. One possible formation scheme of MWCNT/$TiO_2$ hybrid nanostructures is illustrated in Fig. 8.

## 3.6. *Degradation mechanism of MB on MWCNT/$TiO_2$ hybrid nanostructures*

Recently, a few reports indicated that CNTs can act as sensitizers and were excited under visible light irradiation [13,15,41,42]. In the process, the electrons were injected to the conduction band of $TiO_2$ to generate positively charged CNTs, which could capture electrons from the valence band of $TiO_2$, leading to the formation of holes. The electrons and holes further reacted with the absorbed $O_2$ and $H_2O$ to produce active $O_2^-\cdot$ and OH radicals, which were responsible for the

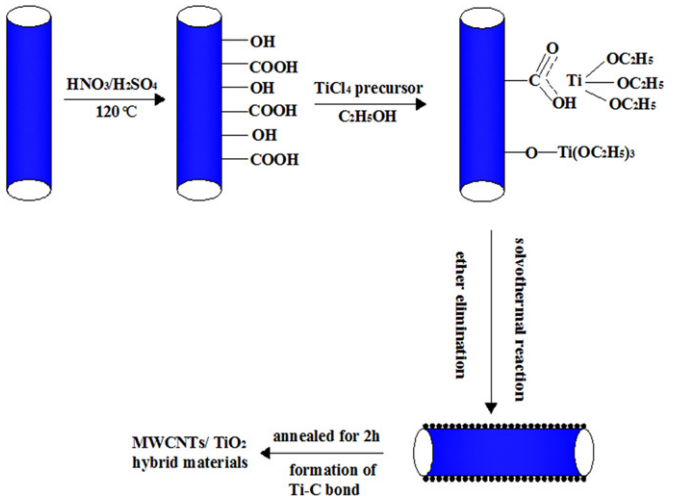


**Fig. 8.** The possible formation scheme of MWCNT/$TiO_2$ hybrid nanostructures in solvothermal condition.

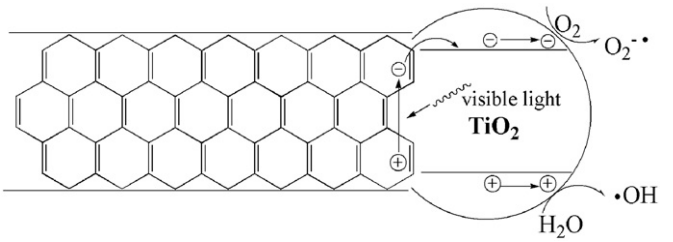


**Fig. 9.** Proposed mechanism of photocatalysis degradation of MB in MWCNT/$TiO_2$ hybrid nanostructures.

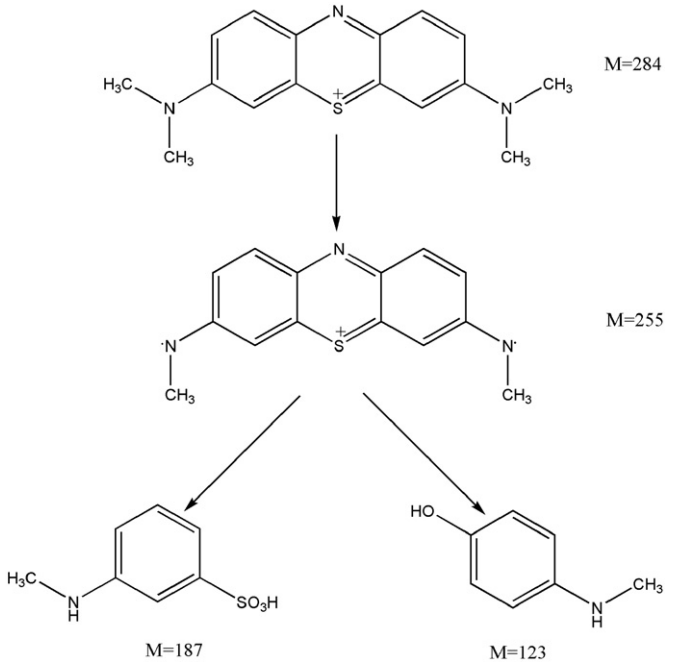


**Fig. 10.** Photocatalytic degradation of MB and intermediate products.

degradation of MB degradation. If we could exclude the influences of the self sensitization of methylene blue, a possible degradation mechanism according to our experimental results and the references [13,15,39] may be like that as shown in Fig. 9. We have to underline that the bonding interaction between the MWCNTs and $TiO_2$, Ti–C bond, is beneficial for electron transfer and extends the absorption of nanostructures in visible light region, which may contribute to the higher photocatalytic degradation of MB in MWCNTs/$TiO_2$ hybrid nanostructures. In addition, the intermediates generated during the degradation process were analyzed by GC/MS and identified by comparison with commercial standards. The sequence of MB bonds breaking, as well as the formation of intermediates, is proposed and presented in Fig. 10. Firstly, MB molecule underwent the demethylation and then the breaking of the MB central aromatic ring containing both heteroatoms, S and N, which was also observed in Yu's investigation by in-situ IR [43]. Subsequently, these intermediates were likely to undergoing the attack of the active $O_2^-\cdot$ or OH radicals and conversed to nontoxic products such as $CO_2$, $H_2O$, $NH_4^+$ and $SO_4^{2-}$ [44].

## 4. Conclusion

In this paper, anatase $TiO_2$ nanoparticles were anchored on CNTs surface via solvothermal method. A comparison was made to evaluate the MWCNT/$TiO_2$ hybrid nanostructures, prepared by sol–gel method and the solvothermal process, respectively. It was found when the weight ratio of CNTs was 20%, the $TiO_2$ nanocrystals decorated on MWCNTs surface uniformly. This morphology facilitated the electron transfer between CNTs and $TiO_2$ and enhanced the photocatalytic activity of hybrid materials. Furthermore, the post-annealing of MWCNT/$TiO_2$ at 400 °C resulted in the formation of Ti–C bonds at the interphase between MWCNTs and $TiO_2$ nanoparticles. The presence of Ti–C bonds extended the light absorption of MWCNT/$TiO_2$ hybrids to the whole visible light region, leading to a higher visible light induced photocatalytic activity.

## Acknowledgments

Financial support by the National Science Foundation of China (No. 20673078), and by open foundation of Key Laboratory of Catalysis and Materials Science of the State Ethnic Affairs Commission and Ministry of Education, South-Central University for Nationalities (No. CHCL06001) are gratefully acknowledged.

## References

[1] A. Fujishima, K. Honda, Nature 238 (1972) 37–38.
[2] A.L. Linsebigler, L. Guanquan, J.T. Yates, Chem. Rev. 95 (1995) 735–758.
[3] M.R. Hoffmann, S.T. Marin, W. Choi, D.W. Bahnemannt, Chem. Rev. 95 (1995) 69–96.
[4] J. Zhu, Z. Deng, F. Chen, J. Zhang, H. Chen, M. Anpo, J. Huang, L. Zhang, Appl. Catal. B: Environ. 62 (2006) 329–335.
[5] H. Tada, T. Mitsui, T. Kiyonaga, T. Akita, K. Tanaka, Nat. Mater. 5 (2006) 782–786.
[6] Z.B. Wu, F. Dong, Y. Liu, H.Q. Wang, Catal. Commun. 11 (2009) 82–86.
[7] J.H. Park, S.W. Kim, A.J. Bard, Nano Lett. 6 (2006) 24–28.
[8] D.C. Hurum, K.A. Gray, T. Rajh, M.C. Thurnauer, J. Phys. Chem. B 109 (2005) 977–980.
[9] T. Ohno, K. Tokieda, S. Higashida, M. Matsumura, Appl. Catal. A: Gen. 244 (2003) 383–391.
[10] M. Stylidi, D.I. Kondarides, X.E. Verykios, Appl. Catal. B: Environ. 47 (2004) 189–210.
[11] A. Kongkanand, P.V. Kamat, ACS Nano 1 (2007) 13–21.
[12] X.H. Peng, J.Y. Chen, J.A. Misewich, S.S. Wong, Chem. Soc. Rev. 38 (2009) 1076–1098.
[13] W.D. Wang, P. Serp, P. Kalck, J.L. Faria, Appl. Catal. B: Environ. 56 (2005) 305–312.
[14] Y. Yu, J.C. Yu, C.Y. Chan, Y.K. Che, J.C. Zhao, L. Ding, W.K. Ge, P.K. Wong, Appl. Catal. B: Environ. 61 (2005) 1–11.
[15] G. An, W. Ma, Z. Sun, Z. Liu, B. Han, S. Miao, Z. Miao, K. Ding, Carbon 45 (2007) 1795–1801.
[16] Y. Yao, G. Li, S. Ciston, R.M. Lueptow, K.A. Gray, Environ. Sci. Technol. 42 (2008) 4952–4957.
[17] L.L. Ma, H.Z. Sun, Y.G. Zhang, Y.L. Lin, J.L. Li, E.K. Wang, Y. Yu, M. Tan, J.B. Wang, Nanotechnology 19 (2008) 115709.
[18] H. Wu, Q. Wang, Y. Yao, C. Qian, X. Zhang, X. Wei, J. Phys. Chem. C 112 (2008) 16779–16783.

[19] K. Byrappa, A.S. Dayananda, C.P. Sajan, B. Basavalingu, M.B. Shayan, K. Saga, M. Yoshimura, J. Mater. Sci. 43 (2008) 2348–2355.
[20] B. Gao, G.Z. Chen, G.L. Puma, Appl. Catal. B: Environ. 89 (2009) 503–509.
[21] Y.J. Xu, Y.B. Zhuang, X.Z. Fu, J. Phys. Chem. C 114 (2010) 2669–2676.
[22] C.Y. Kuo, J. Hazard. Mater. 163 (2009) 239–244.
[23] W.D. Wang, P. Serp, P. Kalck, J.L. Faria, J. Mol. Catal. A Chem. 235 (2005) 194–199.
[24] O. Akhavan, M. Abdolahad, Y. Abdi, S. Mohajerzadeh, Carbon 47 (2009) 3280–3287.
[25] W.T. Yao, S.H. Yu, Adv. Funct. Mater. 18 (2008) 3357–3366.
[26] D.S. Zhang, C.S. Pan, J.P. Zhang, Mater. Lett. 62 (2008) 3821–3823.
[27] E. Elmalem, A.E. Saunders, R. Costi, A. Salant, U. Banin, Adv. Mater. 20 (2008) 4312–4317.
[28] Z. Yu, S.S.C. Chung, Appl. Catal. B: Environ. 83 (2008) 277–285.
[29] D. Eder, A.H. Windle, Adv. Mater. 20 (2008) 1787–1793.
[30] X.H. Xia, Z.J. Jia, Y. Yu, Y. Liang, Z. Wang, L.L. Ma, Carbon 45 (2007) 717–721.
[31] D. Eder, A.H. Windle, J. Mater. Chem. 18 (2008) 2036–2043.
[32] W.D. Zhang, B. Xu, L.C. Jiang, J. Mater. Chem. 20 (2010) 6383–6391.
[33] Y. Huang, W. Ho, S. Lee, L. Zhang, G. Li, J.C. Jimmy, Langmuir 24 (2008) 3510–3516.
[34] L.C. Chen, Y.C. Ho, W.S. Guo, C.M. Huang, T.C. Pan, Electrochim. Acta 54 (2009) 3884–3891.
[35] H. Sun, Y. Bai, Y. Cheng, W. Jin, N. Xu, Ind. Eng. Chem. Res. 45 (2006) 4971–4976.
[36] Z. Song, J. Hrbek, R. Osgood, Nano Lett. 5 (2005) 1327–1332.
[37] K.H. Ji, D.M. Jang, Y.J. Cho, Y. Myung, H.S. Kim, Y. Kim, J. Park, J. Phys. Chem. C 113 (2009) 19966–19972.
[38] H. Yu, X. Quan, S. Chen, H. Zhao, Y. Zhang, J. Photochem. Photobiol. A Chem. 200 (2008) 301–306.
[39] X.H. Wang, J.G. Li, H. Kamiyama, Y. Moriyoshi, T. Ishigaki, J. Phys. Chem. B 110 (2006) 6804–6809.
[40] P.H. Mutin, A. Vioux, Chem. Mater. 21 (2009) 582–596.
[41] K. Woan, G. Pyrgiotakis, W. Sigmund, Adv. Mater. 21 (2009) 1–7.
[42] H.C. Huang, G.L. Huang, H.L. Chen, Y.D. Lee, Thin Solid Films 511/512 (2006) 203–207.
[43] Z. Yu, S.S.C. Chuang, J. Phys. Chem. C 111 (2007) 13813–13820.
[44] A. Houas, H. Lachheb, M. Ksibi, E. Elaloui, C. Guillard, J. Herrmann, Appl. Catal. B: Environ. 31 (2001) 145–157.